A Low-Cost LoRa Optical Fluorometer–Nephelometer for Wireless Monitoring of Water Quality Parameters in Real Time

Soheyl Faghir Hagh, Parmida Amngostar, Wenzhe Chen, Jessica Sheridan, Clayton J. Williams, Ana M. Morales-Williams, Dryver Huston, and Tian Xia, *Senior Member, IEEE*

***Abstract*—The real-time monitoring of water quality parameters using optical sensors has become widespread. However, the price of commercial sensors and the ability to integrate them into customized sensing networks can limit their application in research and monitoring programs. This study introduces the design, verification, and validation of an innovative, low-cost, portable, low-power fluorometer–nephelometer device, employing long-range wide area network technology. The developed Internet of Things capable device can measure temperature, turbidity, phycocyanin fluorescence (a proxy for cyanobacteria biomass), and chlorophyll-*a*(Chl-*a*) fluorescence [a proxy for phytoplankton (cyanobacteria plus algae) biomass] in aquatic ecosystems. The fluorometer–nephelometer structure employs one digital thermistor probe, three distinct light-emitting diodes (LEDs) that are amber (590 nm) to excite phycocyanin pigments of cyanobacteria, blue (465 nm) to excite Chl-*a* pigments of phytoplankton, and near-infrared (NIR) (870 nm) to measure turbidity through light scattering. Two orthogonal silicon photodiodes are used as detectors set in line with long-pass filters of 830 nm for turbidity and 630 nm for phytoplankton. A peristaltic pump circulates water through a polymethylmethacrylate cuvette within a 3-D-printed fluorometer assembled in a weatherproof box. The activation by personalization long range wide area network (LoRaWAN) protocol is utilized for real-time wireless transmission of water quality data, while a micro-SD card is employed for storing the data locally. The optical sensor tests are conducted in the laboratory using standard turbidity solutions and pigments. The turbidity, phycocyanin, and Chl-*a* sensing ranges are 3–200 FTU, 0.025–2.5 mg-PC/L, and 1–50 μg-chl/L, respectively. In repeated laboratory tests, the relative percent difference is consistently less than 10%.**

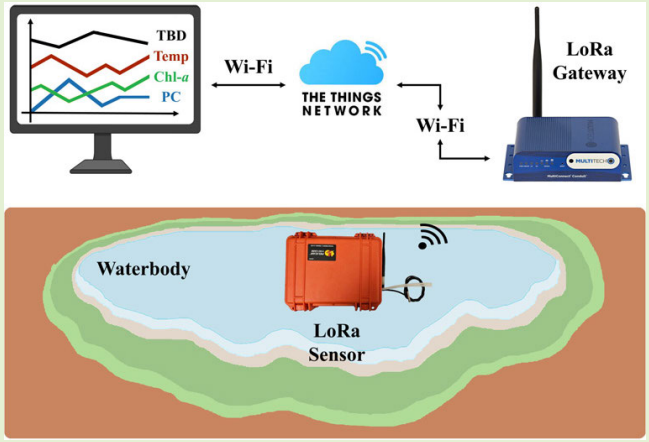

***Index Terms*— Algae, chlorophyll-a (Chl-a), cyanobacteria, Internet of Things, long range wide area network (LoRaWAN), optical sensor, phycocyanin.**

I. Introduction

PHYTOPLANKTON are a diverse group of photosynthetic microorganisms, including eukaryotic algae and procaryotic cyanobacteria, which play a significant role in the aquatic ecosystem food webs and nutrient cycles and the global carbon cycle. While essential for ecosystems as primary producers and mediators of ecosystem structure and function, evidence suggests algae and cyanobacteria overgrowth events (i.e., blooms) have increased in intensity, frequency, and toxicity throughout the Anthropocene [1], [2], [3]. These blooms have substantial negative economic, recreational, public health, and environmental impacts [2], [4]. Climate change and inorganic nutrient pollution from wastewater, agriculture, land use change, industrialization, and urbanization are often credited as the main drivers of blooms [1], [3], [5], but recent evidence suggests that the picture is more complicated. Phytoplankton blooms can also thrive in low-nutrient environments, under cold-water con-

Manuscript received 7 May 2024; accepted 13 May 2024. Date of publication 27 May 2024; date of current version 1 July 2024. This work was supported in part by United States Geological Survey (USGS) under Agreement AWD00000708SUB00000296, in part by Vermont Water Resources and Lakes Studies Center, NSF under Grant 2119485, and in part by the Faculty Development Awards from Saint Michael's College. The associate editor coordinating the review of this article and approving it for publication was Prof. Anindya Nag. *(Corresponding author: Tian Xia.)*

Please see the Acknowledgment section of this article for the author affiliations.

This article has supplementary downloadable material available at https://doi.org/10.1109/JSEN.2024.3403416, provided by the authors.

Digital Object Identifier 10.1109/JSEN.2024.3403416

ditions, and by using organic nutrient pollutants [6], [7], [8]. To better understand the mechanisms by which blooms develop and to protect communities from exposure to blooms and their byproducts, we must expand the spatial and temporal capability to sense phytoplankton within and across aquatic ecosystems and enable rapid data communication to communities.

Phytoplankton biomass, abundance, and potential for toxicity are measured directly or estimated in a variety of ways from laboratory processing of discretely collected water samples to satellite remote sensing. There is not one standard method employed across the world. Still, environmental sensors are an increasingly popular choice to provide time-series data of a single location or discrete sampling-point data within and across waterbodies. Sensor data can be used to estimate phytoplankton biomass and other water quality conditions as well as for ground-truth satellite imagery and ecological hypotheses testing at global scales [9], [10]. Water quality sensor systems can also be used for adaptive management and to issue community-wide alerts about the current conditions of a local waterbody. The problem, however, is that commercially available water quality sensors (both handheld and deployable models) are expensive to purchase and maintain and are often out of reach for researchers, government agencies, and communities with limited resources [11], [12], [13]. Furthermore, commercial sensors and sensing systems often do not communicate wirelessly, rely on proprietary software, or require substantial infrastructure for communication [14], [15]. Hence, the grand challenge of the reliance on sensor systems to monitor water quality is the global availability and accessibility of sensors and the timely transmission and communication of their data to communities directly affected by the environment.

Low-cost, open-source environmental sensors are one way to flatten the system and make sensors and communication networks customizable to the end user's needs and requirements. In addition, low-cost sensor alternatives can provide expanded spatial and temporal coverage of aquatic ecosystems with pre-existing sensor systems and networks. Low-cost sensors can be as technologically sound and reliable (precise, accurate, and durable) as commercially available versions [9], [12], [13], [14], [15], [16], [17]. By integrating sensing, data collection, transmission, visualization, and communication along with customizability, low-cost sensor networks can expand the scope of environmental sensing.

Currently, there exist several low-cost, IoT, and real-time water quality monitoring sensor designs available [12], [13], [14], [15], [16], [17], [18], [19], [20], [21], [22], [23], [24], [25], [26], [27], [28], [29], [30], [31], [32], [33] [34], [34]. However, only a few published designs integrate multiple water quality sensors into a wireless device. Spectrophotometers are developed for water quality monitoring in [12], [15], [17], and [23]. Parra et al. [26], Fay and Nattestad [29], and Wang et al. [30] focus on sensors for measuring water turbidity, while others concentrate on phycocyanin (PC) or chlorophyll-*a* (Chl-*a*) monitoring [18], [19], [20], [32], or fluorometers for laboratory use [21]. Fluorometer designs are available for both PC and Chl-*a* measurements [22]. Some techniques rely on satellite imaging. While satellite imaging offers a remote sensing solution [31], it is an indirect measurement and does not measure water condition parameters. In situ water quality monitoring using uncrewed aerial vehicles (UAVs) has been previously explored as a solution for water sample collection [24], but it does not perform continuous time water sensing.

This work presents a novel wireless multisensor water quality, phytoplankton, and cyanobacteria monitoring system built upon the open-source designs of Porter et al. [21] and Leeuw et al. [18]. Our sensor system incorporates a three-in-one 3-D-printed fluorometer to estimate phytoplankton biomass as Chl-*a* (μg/L) and cyanobacteria abundance as PC (mg/L). Additionally, it integrates a nephelometer to measure water turbidity in Formazin Nephelometric Units (FTU) and a temperature (°C) sensor. This combination results in a user-friendly, portable, low-power, and cost-effective device that can be deployed in a field for wireless monitoring. Our approach employs optical sensors to capture signals from water particles and avoids utilizing chemical reagents. The sensor system transmits water quality data wirelessly to a remote data server and also stores it locally on a micro-SD card for backup. It is adaptable to long range (LoRa) mesh networks, facilitating multiple node deployments across various water bodies or different parts of a water body for extensive monitoring.

The sensor node is housed within an 1150 waterproof case for protecting the electronic circuitry, the three-in-one fluorometer–nephelometer, and batteries from environmental elements, such as water, humidity, and ambient light. Our sensing system is customizable and open source, allowing users to modify it to meet their specific application needs. The system presented in this article can be used for collecting point sample measurements or being deployed for short-term, high-frequency measurements of water conditions at a fixed depth.

The remainder of this article is organized as follows. Section II presents the sensing system architecture and elaborates on different functional units' design and fabrication. Section III presents the laboratory test results for performance validation. Section IV discusses the sensor features and their application values. Section V contains the concluding remarks.

II. Sensing System Architecture

This section provides a detailed description of the design and fabrication processes of our sensing system. It covers the design of the sensing principles and sensor node, encompassing the microprocessor, fluorometer–nephelometer, transimpedance amplifier, and subsequent sensor operation.

A. Fluorometer–Nephelometer Sensing Principles

Phytoplankton are a diverse group of organisms with various photosynthetic pigments and form the food web base in many aquatic ecosystems. In limnology and oceanography fields, the concentration of pigments is commonly used as a surrogate measure of cyanobacteria and algal abundance and biomass [23]. Chl-*a* is the primary photosynthetic pigment of most phytoplankton. The optical intensity of this

pigment is often sensed as an indicator of total phytoplankton biomass, which includes eukaryotic algae and prokaryotic cyanobacteria. Fluorometric analysis, particularly useful for in situ phytoplankton assessment [18], [19], [20], [21], [22], involves artificially exciting Chl-*a* with light wavelength between 400 and 500 nm (deep blue) and measuring the light emission peaks around 670–690 nm (red) released from the phytoplankton cell [18]. Cyanobacteria contain phycobilin assessor pigments, of which PC is most used to sense their abundance in freshwaters. In PC fluorometry methods, light artificially excites PC pigments at around 600 nm (amber) and the light emitted by PC is measured at approximately 650 nm (red) [18]. Turbidity and temperature fluctuations influence the excitation signals, necessitating concurrent measurement with Chl-*a* and PC for enhanced reliability in estimating phytoplankton and cyanobacteria levels.

Water turbidity, reflecting cloudiness and murkiness, results from various biological, mineral, chemical, and optical properties of particles and dissolved solids within aquatic environments. To distinguish emitted or reflected light signals from particles in water, a near-infrared (NIR) light source is developed, which minimizes light absorbance within the water matrix. Our nephelometer employs an 870-nm NIR LED for turbidity detection via 90° light scattering by particles in water samples [25]. This method is effective across clear and turbid waters. Like phytoplankton, turbidity signals are influenced by water temperature variations due to their impacts on water's optical properties. Hence, the simultaneous measurement of temperature alongside turbidity is essential for accurate assessment.

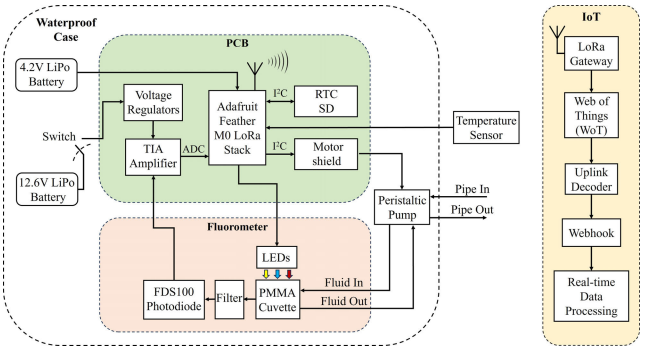

Fig. 1. IoT-capable water quality sensor system block diagram. The electronics are assembled inside the waterproof case.

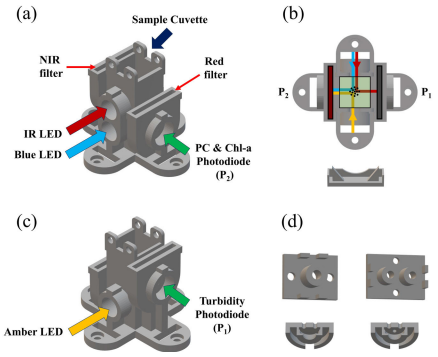

Fig. 2. Fluorometer–nephelometer CAD structure with NIR, blue, and amber LEDs, filters, and holders. (a) 45° angle front side view. (b) Top view and filter holder cap: illustrates the paths of incident light and 90° scattered light as they interact with the suspended particles and cells in the sample inside the cuvette. (c) 45° angle backside view. (d) Photodiode and LED holders: two top pieces are for LED housing and two bottom halves are for enclosing the FDS100 photodiodes.

B. Sensor Node Components

As Fig. 1 shows, the sensor node electronics centers on an Adafruit Feather M0, integrating an RFM95 LoRa transceiver and an ATSAMD21G18 ARM Cortex M0 processor clocked at 48 MHz. It utilizes an Adafruit motor shield to drive a peristaltic pump and includes additional components, such as a real-time clock (RTC) and a micro-SD card module. Two LEDs LED590L and LED450L are used to excite PC and Chl-*a* pigments and their light emissions, while a nephelometer measures light scatter from particles using an LED870L LED. All emissions are detected at a 90° angle perpendicular to the LED light source. All LEDs are sourced from Thorlabs Inc. (NJ, USA).

C. Fluorometer–Nephelometer Fabrication

The CAD design illustrated in Fig. 2 presents a multifunctional fluorometer–nephelometer with dual orthogonal incident light paths for each photodetector. Fig. 2(a) and (c) outlines the device's structure, while Fig. 2(b) illustrates light paths and sample positioning within the polymethyl methacrylate (PMMA) cuvette. Fig. 2(d) showcases LED and photodiode holders. To counter interference from background red-light wavelengths on the fluorometer photodiode (P_2), a Thorlabs Inc. FGL630 red glass long-pass filter is used. An FGL830 infrared glass long-pass filter is employed for the nephelometer detector (P_1). The PMMA cuvette is modified into a flowthrough cell by removing its bottom, and 3-D-printed tube barb caps are attached to each end using marine epoxy. These components are 3-D-printed using polylactic acid (PLA) filaments.

D. Circuit Design and Fabrication

The sensor node printed circuit board (PCB) consists of the microcontroller stack, three complementary metal–oxide–semiconductor (CMOS) drivers, each for one LED, a DS18B20 waterproof digital temperature sensor (Adafruit Industries), and two low-noise transimpedance amplifiers (TIAs).

1) Power Supply: The power supply system, depicted in Fig. S1 (in the supplemental document), comprises a CMOS power switch, linear voltage regulators, and a resistive divider. It generates a 5-V source for LEDs, a 9-V voltage source for precision operational amplifiers, and a 3.3-V voltage source for the feedback multiplexer (MUX) and temperature sensor. The resistive divider's output (CAP) monitors the main battery voltage using an analog-to-digital converter (ADC) pin.

2) Transimpedance Amplifiers: TIAs are pivotal in our sensing system, converting photodiode currents to measurable voltages. This step is crucial due to photodiodes' current being proportional to incident light intensity. As the current amplitude is very small, it poses big challenges for

TABLE I
FLUOROMETER AND NEPHELOMETER TIA DESIGN PARAMETERS

Parameter	Fluorometer-H[a]	Fluorometer-L[b]	Nephelometer
$I_{In,\,Max}$ (nA)	1.8	9	900
$I_{In,\,Min}$ (A)	0	0	0
$V_{O,\,Max}$ (V)	9	9	9
$V_{O,\,Min}$ (V)	0	0	0
Gain (V/A)	5G	1G	10M

[a]High sensitivity channel of the transimpedance amplifier.
[b]Low sensitivity channel of the transimpedance amplifier.

direct measurement. Precision operational amplifiers utilizing OPA191 amplify photodiode currents. The amplifiers for the fluorometer and nephelometer are configured for their specific needs, with the nephelometer featuring a fixed *RC* network (Fig. S2) and the fluorometer employing a variable feedback *RC* network (Fig. S3) for resolution adjustment. The SAMD M0 microprocessor's 10-bit ADC measures the TIAs' output voltage with a stable 3.3-V reference voltage. The detailed design characteristics are summarized in Table I.

The TIAs' design process involves calculating the feedback resistor (R_F) using (1) and the maximum allowable feedback capacitor (C_F) using (2). In (1), $V_{O,Max}$, and $V_{O,Min}$ determine the desired output voltage range for the op-amps

$$R_F = (V_{O,Max} - V_{O,Min})/I_{in,Max} \tag{1}$$

$$C_F \leq (2\pi R_F f_{-3\,db})^{-1} \tag{2}$$

where $f_{-3\,db}$ is the pole frequency (cutoff frequency) set by the *RC* feedback network. Equations (3) and (4) ensure amplifier stability and suitable op-amp selection

$$f_{GBW} > (C_{IN} + C_F)/\left(2\pi R_F C_F^2\right) \tag{3}$$

$$C_{IN} = C_J + C_D + C_{CM}. \tag{4}$$

The photodiode junction capacitance is C_J (24 pF for FDS100), the op-amp's differential input capacitance (C_D) is 1.6 pF, and the common-mode input capacitance of the amplifier (C_{CM}) is 6.4 pF. Using (3), the chosen op-amp must have an $f_{GBW} > 237$ KHz for the nephelometer–fluorometer. The op-amp outputs have a saturation voltage of 9 V.

Since the 10-bit ADC of M0 operates at a 3.3-V logic level, the output voltages for both TIAs are adjusted using a low-power voltage divider to match these levels. Additionally, a 1-μF capacitor (C_{out}) is employed for noise attenuation. The dc output voltage is determined by the following:

$$V_{out} = (R_F I_{Photo}) \times (R_2/(R_1 + R_2)). \tag{5}$$

The TIA circuit for PC and Chl-*a* photodiodes, as depicted in Fig. S3, incorporates an *RC* network selector multiplexer with input (IN) and enable (EN) pins for control. This functionality is utilized for resolution selection. Table II provides the truth table for *RC* selection.

3) LED Drivers, Pump Switch, and Temperature Sensor: Each LED has a 100-Ω series resistor and a driver in Fig. S4(a). The temperature sensor requires a 4.7-Ω pull-up resistor on the data bus in Fig. S4(b). The pump switch functions as a current source switch because of the motor shield's active low logic in Fig. S4(c).

TABLE II
TRUTH TABLE FOR RESOLUTION SELECTION

EN	IN	OP1	OP2	Function
1	X	High-Z	High-Z	Disabled
0	0	L1	L3	High-res.
0	1	L2	L4	Low-res.

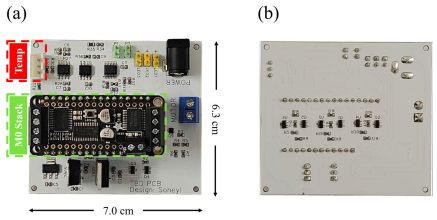

Fig. 3. Fabricated double-sided sensor node PCB. (a) Top view. (b) Bottom mirrored view.

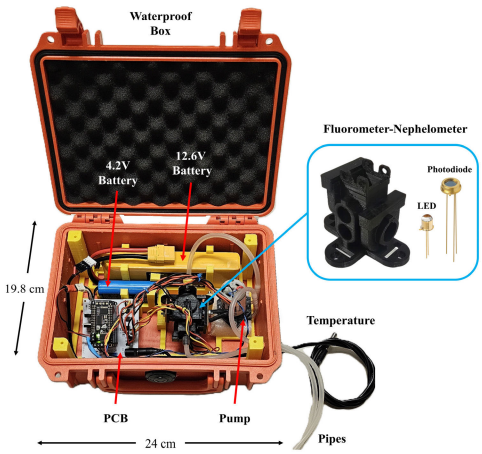

Fig. 4. LoRa Fluorometer–nephelometer waterproof box assembly.

4) PCB Fabrication: The PCB, Fig. 3, contains all the components, including the microprocessor stack (M0, RTC, and motor shield modules), TIAs, drivers, and switches. The 1.6-mm-thick double-sided PCB is manufactured using surface-mount circuit components with FR-4 material. The simulated PCB is provided in Fig. S5.

5) Sensor Box Assembly: The sensor node is housed within a Pelican[1] 1150 case, depicted in Fig. 4, and secured to a 3-D-printed frame (yellow frame). Inside the case, there are two lithium-polymer (LiPo) batteries, one with a voltage of 12.6 V (for the PCB) and the other with 4.2 V (for the M0 microcontroller). Additionally, the temperature sensor and input/output pipes are mounted on the side of the case.

Fig. S6 presents a flowchart illustrating the sensing sequence. The sensing process starts with the connection of both batteries (main PCB power and M0), followed by the initialization of modules, including the RTC module and the motor shield. After a brief 5-s delay, the M0 triggers the CMOS power switch shown in Fig. S1, powering up all components of the PCB, and initiating the fluid pumping into the cuvette and sample analysis.

[1]Trademarked.

TABLE III
COMPONENT POWER CONSUMPTION

Component list	Active current (mA)	Sleep current (mA)	Active Power (mW)
Temp. sensor	1.5	0	7.5
LED590L	30	0	60
LED450L	40	0	40
LED870L	32.8	0	56.41
Pump	467	0	2,802
Feather M0	120 (Tx)	18.2	396
Total	691.3	18.2	3361.91

6) Power Consumption: In our design, we utilize a 12.6-V battery for the circuit and a separate 4.2-V battery for the Feather M0 stack, extending the sensor node's overall operational life. A main CMOS switch (Fig. S1) disconnects components during sleep mode to conserve power. Refer to Table III for component power consumption. The operational duty cycle includes 5-s activation of LEDs, 7-s pump activation, 5-s data transmission (TX), and 15 min of sleep time. Because of the low activation duty cycle, the overall energy consumption remains low.

E. LoRaWAN Technology

LoRa is a type of low-power wide area network (LPWAN) wireless communication technology designed to transmit small data packets over long distances while operating on low battery power. It utilizes a proprietary spread spectrum modulation scheme based on chirp spread spectrum (CSS) modulation, allowing for efficient long-range communication. LoRa wide area network (LoRaWAN) is the protocol layer built on LoRa, enabling bidirectional communication between end nodes and gateways [34]. This technology enables wireless transmission of water quality data from field-deployed fluorometer–nephelometers to a LoRa gateway station to forward data packets to the cloud. In this project, LoRa communication is set up via a 915-MHz Adafruit Feather M0 LoRa end node, registered on The Things Network (TTN) server using the Activation by Personalization (ABP) protocol for efficiency. Our tests show that the ABP protocol is more efficient than the Over the Air Activation (OTAA) method, as it skips the joining procedure required with OTAA, reducing the time by about 1 min for a network rejoining. Session keys (NwkSKey and AppSKey) and device address (DevAddr) are stored in nonvolatile memory on the end device (Feather M0). The frame counter is manually reset upon sensor node deployment. Data transmission occurs every 15 min at +20-dBm transmission power, achieving a maximum distance of around 0.8 km in urban areas.

F. On-Chip Signal Processing and Wireless Transmission

Algorithm 24 outlines the sampling and wireless data transmission processes in Arduino code format. It initializes variables for data management and LoRa transmission setup using the LMIC library. The setup section includes functions for LoRa transmission, pump control, and photodiode readings. In the main loop, a single iteration of the LMIC event loop is executed, sensor data are collected, and sleep mode is managed. Sampling involves activating LEDs for 5 s for stability and taking 100 photodiode readings, from which mean and standard deviation are calculated ON-chip. Data are encoded into a 14-byte payload, with each parameter split into high and low bytes for transmission. The packet includes seven parameters, including temperature, turbidity, battery voltage, PC (high and low), and Chl-*a* (high and low).

Algorithm 1 Arduino Program for the LoRa Fluorometer–Nephelometer

```
Define variables: uint_8 data [14], osjob_t sendjob, int16_t int16_Sensor.
Setup:
    Initialize modules and configure pin modes and mappings.
Function 1: do_send (osjob_t* j)
    data [k] = (byte) (int16_Sensor ≫ 8)
    data [k+1] = (byte) (int16_Sensor & 0x00FF)
    LMIC_setTxData2 (7, data, 14, 0)
Function 2: Pump (mode, speed)
    Input: Pumping modes such as in, out, idle, and pumping speed.
    Motor shield ← run (mode), setSpeed (speed).
Function 3: Get_data ()
    Read the time, date, battery voltage, and temperature.
    Turn on the corresponding LED using analogWrite (LED, 255).
    Set the resolution using IN and EN for PC and Chl-a channels.
    for (j = 0; j < 100; j ← j + 1)
        AccValue ← AccValue + analogRead (TIA)
        Sensor [j] ← analogRead (TIA)
    end
    Turn off the LED and calculate average int16_Sensor values.
    Store data to SD card and transmit it using do_send (&sendjob).
Loop:
    Activate the CMOS power switch and execute os_runloop_once ().
    Pump fluid in, Get_data (), pump fluid out.
    Turn off the power switch and go to sleep (15 minutes).
```

G. Cloud Data Management and IoT

The IoT platform depicted in Fig. 5 comprises the end device (sensor box), the LoRa gateway (transceiver), the Web of Things (The Things Stack), and a webhook (Datacake website). The RFM95 LoRa module in class A LoRaWAN transmission mode has a bandwidth of 125 KHz. The water quality data are collected every 15 min, and the 14-byte data array requires approximately 14 s of transmission time. The MultiTech Conduit gateway is connected to the cloud via Wi-Fi, and it receives the uplink from the end node and relays it to TTN server. From there, it is directed to the Datacake

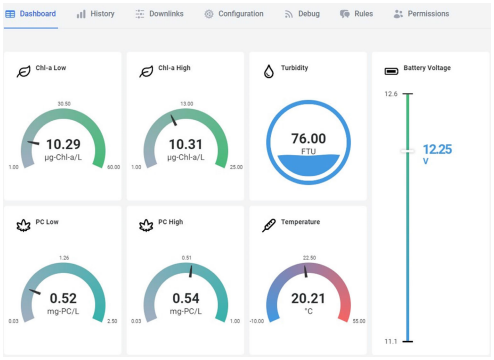

Fig. 5. Datacake IoT platform for on-cloud data management.

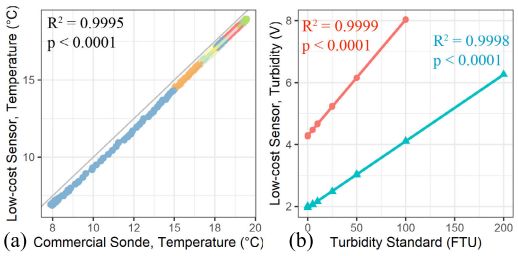

Fig. 6. (a) Temperature comparison between low-cost sensor system and commercial sonde (black line is linear smooth, and gray line is 1:1). (b) Low-cost turbidity channel response at room temperature to standard reference matter using a 3-mm-diameter LED aperture and 4-mm-diameter LED aperture.

webhook and decoded into individual bytes using a JavaScript decoder. It starts by extracting battery voltage from the first two bytes of the payload and then interprets the next two bytes as a temperature value, considering a signed value followed by two bytes for turbidity. Finally, it decodes four bytes for PC (high and low) and four for Chl-*a* (high and low).

III. Results and Sensor Validation

This section describes the calibration and testing of sensors for measuring water quality parameters, including temperature, turbidity, PC, and Chl-*a* sensors. It also shows the data management on the data server.

A. Experimental Test Bench

This part provides details regarding all sensor tests and the test bench setup.

The low-cost temperature sensor is tested for 12 days alongside a commercial Aqua TROLL 500 sensor. Measurements are taken every 15 min using two setups. The first involves a 20-gallon aquarium filled with tap water, initially cooled with eight freezer packs. After 48 h, a new set of packs is used. The aquarium is incubated in low light. The second setup uses a 1-gallon container on a window ledge, which is exposed to direct sunlight and induces diurnal temperature changes.

Turbidity, PC, and Chl-*a* testing are conducted at room temperature (19 °C) under low light. Fresh standards are prepared weekly, and the sensor is sampled every 10 s. Pump tubing is cycled through standards starting with the lowest and mixed before each sampling. After measuring the highest standard, the system is rinsed with deionized water for three cycles. Battery charging maintains consistent power levels. Testing spans two weeks.

Chl-*a* standards are made by extracting Spinach in methanol for 24 h at −20 °C, followed by filtering extract through a 0.7 μm glass fiber filter. The concentration is then determined using a spectrophotometric method [35]. Phycocyanin standards are made using freeze-dried *Spirulina* nutritional supplements (Blue *Spirulina*, 35% phycocyanin, Double Wood Supplements). Rhodamine WT working standards (0–2000 μg/L), a secondary dye standard that is more stable and affordable than pigment standards, were made from 2.5% manufactured stock solution by serial dilution.

Working turbidity standards (0–200 FTU) are made by serial dilutions of a 1000 FTU Formazine manufactured stock solution. Turbidity tests are conducted with two LED aperture sizes (3 and 4 mm). Altering the aperture size allows for sensitivity adjustment without changing the electronics, which enables the sensing system to work within a wider range of environmental conditions common to wetlands, ponds, and shallow lakes.

B. Temperature and Turbidity Calibration

Temperature tests range from 7 °C to 20 °C, with both low-cost and commercial sensors showing similar responses in Fig. 6(a). They correlate strongly ($R^2 = 0.9995$) with a slope close to 1.01. However, a significant y-intercept difference indicated an average deviation of 0.75 °C between their measurements. Our sensor offers ±0.5 °C accuracy, while the commercial one provides ±0.1 °C. Despite the deviation, the strong linear relationship suggests reliable correction for magnitude differences.

In the low-cost turbidity sensor test, both aperture sizes show a linear response across the working standard set, with R^2 values of 0.9998 for 3-mm aperture and 0.9999 for 4-mm aperture [Fig. 6(b)]. The 3-mm aperture exhibits a lower blank voltage (1.96 V) and can detect up to 200 FTU before saturation, whereas the 4-mm aperture saturates just over 100 FTU but offers better sensitivity (1 FTU compared to 3 FTU). Our turbidity sensor's performance is suitable for typical wetland, pond, and lake environments with their turbidity levels being below 200 FTU. Additionally, it is unaffected by dissolved pigments, watercolor, and dyes, indicating that the signal is solely influenced by the amount and density of the suspended solids in the water.

C. Phycocyanin Detection and Calibration

The cyanobacteria sensor response is tested using two pigment standards (Chl-*a* and PC), a secondary standard (Rhodamine WT), and a turbidity standard. The PC and Chl-*a* sensors use a transimpedance amplifier (Fig. S3) to select detection resolutions via logic values for EN and IN pins (Table II). The cyanobacteria sensor responds linearly to all standards at both detection resolutions (R^2 range is from 0.9638 to 0.9987 in Fig. 7). Chl-*a* standard signal indicates nontarget pigment interference, while the turbidity standard signal represents parasitic wavelengths from the amber LED scattering off Formazine particles. These interferences can

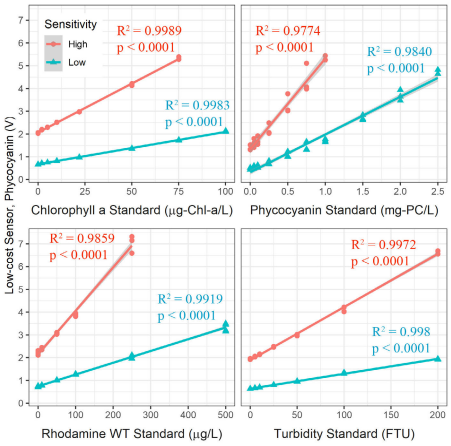

Fig. 7. Response of phycocyanin (PC) sensor to four standard materials. This sensor channel targets rhodamine WT and phycocyanin standards. Turbidity and Chl-*a* standards are parasitic signals from the LED that can be mathematically corrected in this channel.

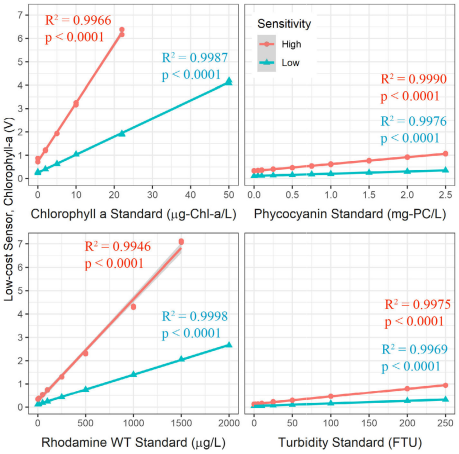

Fig. 8. Response of Chl-a sensor to four standard materials. This sensor channel targets rhodamine WT and Chl-*a* standards. Turbidity and phycocyanin standards are parasitic signals from the LED that can be mathematically corrected in this channel.

be corrected in the target pigment voltage by accounting for additional voltage caused by turbidity-induced light scatter and nontarget pigment. Considering these nontarget and parasitic signals, the cyanobacteria sensor has a detection range of 0.025–2.5 mg-PC/L for turbidity $\leq$ 100 FTU.

D. Chlorophyll-a Detection and Calibration

The phytoplankton biomass sensor response is tested using the same standard sets as the cyanobacteria sensor. The Chl-*a* sensor shares the same amplifier as the PC; hence, the MUX switch selects two resolutions. This sensor responds linearly to all standards at both detection resolutions ($R^2 \geq$ 0.9946 in Fig. 8). Target standards for phytoplankton biomass are Chl-*a* and rhodamine WT. The phytoplankton biomass sensor is only weakly impacted by nontarget pigment (PC) interference. Nontarget signal interference is less than 0.1 V when PC is below 1 and 0.25 mg-PC/L for low and high resolution, respectively. At these interference levels, PC will only meaningfully interfere with total phytoplankton biomass estimations during very dense cyanobacteria blooms. Similarly, the parasitic blue LED signal caused by increasing turbidity and light scattering is weak and does not impact target voltage below 25 and 50 FTU for high and low sensitivity, respectively. Hence, the phytoplankton signal is reliable in most situations without correction and has a biomass detection range of 1–50 μg-Chl-*a*/L when turbidity $\leq$ 250 FTU.

IV. Discussion

This study presents the design and functionality of a fully customizable sensor and communication system. Our low-cost, portable, low-power fluorometer–nephelometer device functions well within commonly observed ranges of temperature, turbidity, cyanobacteria, and phytoplankton in aquatic systems. The sensor system responds linearly to target standards with a relative difference of 10%. Interference from nontarget signals and parasitic LED wavelengths is minimal for turbidity and phytoplankton biomass sensors and within correctable limits for the cyanobacteria sensor. Excluding labor, the sensor system tested in this study costs approximately US$367. The system can be used for field or laboratory measurements of discretely collected water samples or deployed at the surface of an aquatic ecosystem for short-term continuous monitoring. With the LoRaWAN system and enabled IoT, information can be transmitted wirelessly in real time to allow adaptive management of ecosystems and for recreation to inform the public about the current water conditions in real time.

The sensor system presented in this study is designed and customized for low to moderate-nutrient wetlands, ponds, and lakes that experience episodic phytoplankton and cyanobacteria blooms. It has detection ranges of 3–200 FTU for turbidity, 0.025–2.5 mg-PC/L for cyanobacteria, and 1–50 μg-Chl-*a*/L for phytoplankton biomass. As depicted in Table IV, the detection ranges of our sensor system expand upon the range and capabilities reported by Leeuw et al. [18] (the original design) and that of a smartphone image detector (SmartFluo in [20]) and an OceanOptics detector-based submersible LED sensor system [19]. Our system enhances low-cost or custom designs by integrating multiple sensors. While direct comparison is challenging due to cyanobacteria's lack of standard units, our system can detect levels within and below World Health Organization guidelines [23]. Our sensor system saturates when guidelines are exceeded. Yet, the combination of turbidity and phytoplankton sensors can still alert about potentially hazardous water quality conditions.

Our sensor system features a peristaltic pump to draw water into a dark flow cell. The flow cell is designed to block ambient light from the sample. Additionally, our system offers internal data logging like commercial sensors, along with wireless transmission for real-time monitoring of water quality parameters. It provides reliable detection, accuracy, and precision at a fraction of the cost of commercial systems.

This sensor system design is highly adaptable, following an open-source approach. For instance, in environments with high nutrient levels causing algal and cyanobacteria blooms, resistance can be adjusted for less sensitive estimations. In river deployments, turbidity gain adjustments or adding

TABLE IV
COMPARISON BETWEEN OUR SENSOR SYSTEM AND THE LITERATURE

Features and Sensors	This Study[a]	Power [32]	Krkljes [33]	Shin [22]	Goblirsch [36]
Temp. (°C)	-5–50	N/A	-40–125	N/A	-40–125
Chlorophyll-*a* (μg/L)	1–50	1–20	N/A	250–5,000	N/A
Phycocyanin (mg/L)	0.025–2.5	N/A	N/A	250–5,000	N/A
Turbidity (FTU-NTU-FNU)	3–200	N/A	0–500	N/A	0.2–40
Conductivity (μS/m)	N/A*	N/A	0–1000	N/A	N/A
Wireless	✓	X	✓	X	✓

[a,*] The proposed sensor system in this work has the capability of integrating additional sensors such as conductivity.

a turbidimeter-capable detector could be considered. Also, changing the LED aperture diameter in Fig. 2(d) alters system sensitivity. While the current design samples at a fixed depth, adding extra motors could enable the intake tube to move through the water column, providing the estimates of conditions at multiple depths. Overall, the design is robust and easily customizable to meet specific user needs.

V. CONCLUSION

Our sensor system integrates a 3-D-printed fluorometer–nephelometer, LoRa technology, and peristaltic pump to monitor phytoplankton biomass, cyanobacteria levels, water clarity, and temperature in a user-friendly portable, low-power, and low-cost wireless device. This sensor system is customizable and reliable and significantly advances its applicability across early detection of harmful algal blooms in recreational waters, ongoing surveillance of drinking water sources, academic research, and long-term ecological studies investigating the impact of environmental factors on aquatic biodiversity. Additionally, it is suitable for deployment in remote or challenging-to-access locations.

The limitations of the system are the LoRaWAN communication range, sensor sensitivity to sediments and biofouling in the cuvette, and the limited battery life. These limitations could be improved by adjusting the spread factor (SF) and transmission power, replacing the sample cuvette on time, utilizing solar panels alongside the sensor box for improved battery time, and utilizing low-power pumps accordingly.

Future work involves the deployment of several sensor boxes in the field for continuous monitoring of algal blooms in addition to water quality and incorporating the fluorometer–nephelometer boxes into a smart IoT LoRa network.

ACKNOWLEDGMENT

Soheyl Faghir Hagh, Parmida Amngostar, Wenzhe Chen, and Tian Xia are with the Department of Electrical Engineering, University of Vermont, Burlington, VT 05405 USA (e-mail: sfaghirh@uvm.edu; Parmida.amngostar@uvm.edu; wenzhe.chen@uvm.edu; txia@uvm.edu).

Jessica Sheridan is with the Department of Civil and Environmental Engineering, University of Vermont, Burlington, VT 05405 USA (e-mail: jesssheridan04@gmail.com).

Clayton J. Williams is with the Department of Environmental Studies and Science, Saint Michael's College, Colchester, VT 05439 USA (e-mail: cwilliams8@smcvt.edu).

Ana M. Morales-Williams is with the Rubenstein School of Environmental and Natural Resources, University of Vermont, Burlington, VT 05405 USA (e-mail: Ana.Morales@uvm.edu).

Dryver Huston is with the Department of Mechanical Engineering, University of Vermont, Burlington, VT 05405 USA (e-mail: dryver.huston@uvm.edu).

REFERENCES

[1] Z. E. Taranu et al., "Acceleration of cyanobacterial dominance in north temperate-subarctic lakes during the anthropocene," *Ecology Lett.*, vol. 18, no. 4, pp. 375–384, Apr. 2015, doi: 10.1111/ele.12420.

[2] X. Hou et al., "Global mapping reveals increase in lacustrine algal blooms over the past decade," *Nature Geosci.*, vol. 15, no. 2, pp. 130–134, Feb. 2022, doi: 10.1038/s41561-021-00887-x.

[3] A. J. Heathcote, Z. E. Taranu, N. Tromas, M. MacIntyre-Newell, P. R. Leavitt, and F. R. Pick, "Sedimentary DNA and pigments show increasing abundance and toxicity of cyanoHABs during the anthropocene," *Freshwater Biol.*, vol. 68, no. 11, pp. 1859–1874, Nov. 2023, doi: 10.1111/fwb.14069.

[4] B. W. Brooks et al., "Are harmful algal blooms becoming the greatest inland water quality threat to public health and aquatic ecosystems?" *Environ. Toxicol. Chem.*, vol. 35, no. 1, pp. 6–13, Jan. 2016, doi: 10.1002/etc.3220.

[5] A. M. Morales-Williams, A. D. Wanamaker, C. J. Williams, and J. A. Downing, "Eutrophication drives extreme seasonal CO_2 flux in lake ecosystems," *Ecosystems*, vol. 24, no. 2, pp. 434–450, Mar. 2021, doi: 10.1007/s10021-020-00527-2.

[6] K. L. Reinl et al., "Cyanobacterial blooms in oligotrophic lakes: Shifting the high-nutrient paradigm," *Freshwater Biol.*, vol. 66, no. 9, pp. 1846–1859, Sep. 2021, doi: 10.1111/fwb.13791.

[7] K. L. Reinl et al., "The role of organic nutrients in structuring freshwater phytoplankton communities in a rapidly changing world," *Water Res.*, vol. 219, Jul. 2022, Art. no. 118573, doi: 10.1016/j.watres.2022.118573.

[8] K. L. Reinl et al., "Blooms also like it cold," *Limnol. Oceanogr. Lett.*, vol. 8, no. 4, pp. 546–564, Aug. 2023, doi: 10.1002/lol2.10316.

[9] F. Mao, K. Khamis, S. Krause, J. Clark, and D. M. Hannah, "Low-cost environmental sensor networks: Recent advances and future directions," *Frontiers Earth Sci.*, vol. 7, p. 221, Sep. 2019, doi: 10.3389/feart.2019.00221.

[10] K. Zolfaghari et al., "Impact of spectral resolution on quantifying cyanobacteria in lakes and reservoirs: A machine-learning assessment," *IEEE Trans. Geosci. Remote Sens.*, vol. 60, 2022, Art. no. 5515520, doi: 10.1109/TGRS.2021.3114635.

[11] J. A. A. Pascua, A. J. A. Prado, B. R. B. Solis, A. P. Cid-Andres, and C. J. B. Cambiador, "Trends in fabrication, data gathering, validation, and application of molecular fluorometer and spectrofluorometer," *Spectrochimica Acta A, Mol. Biomolecular Spectrosc.*, vol. 220, Sep. 2019, Art. no. 116837, doi: 10.1016/j.saa.2019.02.061.

[12] M. W. Prairie, S. H. Frisbie, K. K. Rao, A. H. Saksri, S. Parbat, and E. J. Mitchell, "An accurate, precise, and affordable light emitting diode spectrophotometer for drinking water and other testing with limited resources," *PLoS ONE*, vol. 15, no. 1, Jan. 2020, Art. no. e0226761, doi: 10.1371/journal.pone.0226761.

[13] D. Dwivedi et al., "Biogeosciences perspectives on integrated, coordinated, open, networked (ICON) science," *Earth Space Sci.*, vol. 9, no. 3, Mar. 2022, Art. no. e2021EA002119, doi: 10.1029/2021ea002119.

[14] C. Varadharajan et al., "Challenges in building an end-to-end system for acquisition, management, and integration of diverse data from sensor networks in watersheds: Lessons from a mountainous community observatory in east river, Colorado," *IEEE Access*, vol. 7, pp. 182796–182813, 2019, doi: 10.1109/ACCESS.2019.2957793.

[15] Q. Quevy, M. Lamrini, M. Chkouri, G. Cornetta, A. Touhafi, and A. Campo, "Open sensing system for long term, low cost water quality monitoring," *IEEE Open J. Ind. Electron. Soc.*, vol. 4, pp. 27–41, 2023, doi: 10.1109/OJIES.2022.3233919.

[16] O. Mendoza-Cano et al., "Experiments of an IoT-based wireless sensor network for flood monitoring in colima, Mexico," *J. Hydroinformatics*, vol. 23, no. 3, pp. 385–401, May 2021, doi: 10.2166/hydro.2021.126.

[17] L. D. Alejandrino, J. J. D. Jocson, M. R. R. Mirarza, E. D. Dimaunahan, R. G. Garcia, and F. L. Valiente, "IoT-based estimation system for microcystis aeruginosa cyanobacteria in Laguna de bay using an arduino-controlled spectrophotometric device," *E3S Web Conferences*, vol. 325, p. 04007, 2021, doi: 10.1051/e3sconf/202132504007.

[18] T. Leeuw, E. Boss, and D. Wright, "In situ measurements of phytoplankton fluorescence using low cost electronics," *Sensors*, vol. 13, no. 6, pp. 7872–7883, Jun. 2013, doi: 10.3390/s130607872.

[19] A. Puiu, L. Fiorani, I. Menicucci, M. Pistilli, and A. Lai, "Submersible spectrofluorometer for real-time sensing of water quality," *Sensors*, vol. 15, no. 6, pp. 14415–14434, Jun. 2015, doi: 10.3390/s150614415.

[20] A. Friedrichs, J. Busch, H. van der Woerd, and O. Zielinski, "SmartFluo: A method and affordable adapter to measure chlorophyll a fluorescence with smartphones," *Sensors*, vol. 17, no. 4, p. 678, Mar. 2017, doi: 10.3390/s17040678.

[21] L. A. Porter, C. A. Chapman, and J. A. Alaniz, "Simple and inexpensive 3D printed filter fluorometer designs: User-friendly instrument models for laboratory learning and outreach activities," *J. Chem. Educ.*, vol. 94, no. 1, pp. 105–111, Jan. 2017, doi: 10.1021/acs.jchemed.6b00495.

[22] Y.-H. Shin, J. Z. Barnett, M. T. Gutierrez-Wing, K. A. Rusch, and J.-W. Choi, "A hand-held fluorescent sensor platform for selectively estimating green algae and cyanobacteria biomass," *Sens. Actuators B, Chem.*, vol. 262, pp. 938–946, Jun. 2018, doi: 10.1016/j.snb.2018.02.045.

[23] A. V. Agberien and B. Örmeci, "Monitoring of cyanobacteria in water using spectrophotometry and first derivative of absorbance," *Water*, vol. 12, no. 1, p. 124, Dec. 2019, doi: 10.3390/w12010124.

[24] S. F. Hagh et al., "Autonomous UAV-mounted LoRaWAN system for real-time monitoring of harmful algal blooms (HABs) and water quality," *IEEE Sensors J.*, vol. 24, no. 7, pp. 11414–11424, Apr. 2024, doi: 10.1109/JSEN.2024.3364142.

[25] *ISO 7027-1:2016*. Accessed: Feb. 8, 2024. [Online]. Available: https://www.iso.org/standard/62801.html

[26] L. Parra, A. Ahmad, S. Sendra, J. Lloret, and P. Lorenz, "Combination of machine learning and RGB sensors to quantify and classify water turbidity," *Chemosensors*, vol. 12, no. 3, p. 34, Feb. 2024, doi: 10.3390/chemosensors12030034.

[27] S. Geetha and S. Gouthami, "Internet of Things enabled real time water quality monitoring system," *Smart Water*, vol. 2, no. 1, pp. 1–19, Dec. 2016, doi: 10.1186/s40713-017-0005-y.

[28] D. R. Prapti, A. R. M. Shariff, H. C. Man, N. M. Ramli, T. Perumal, and M. Shariff, "Internet of Things (IoT)-based aquaculture: An overview of IoT application on water quality monitoring," *Rev. Aquaculture*, vol. 14, no. 2, pp. 979–992, Mar. 2022, doi: 10.1111/raq.12637.

[29] C. D. Fay and A. Nattestad, "Advances in optical based turbidity sensing using LED photometry (PEDD)," *Sensors*, vol. 22, no. 1, p. 254, Dec. 2021, doi: 10.3390/s22010254.

[30] Y. Wang, S. M. S. M. Rajib, C. Collins, and B. Grieve, "Low-cost turbidity sensor for low-power wireless monitoring of fresh-water courses," *IEEE Sensors J.*, vol. 18, no. 11, pp. 4689–4696, Jun. 2018, doi: 10.1109/JSEN.2018.2826778.

[31] A. S. P. Pamula, H. Gholizadeh, M. J. Krzmarzick, W. E. Mausbach, and D. J. Lampert, "A remote sensing tool for near real-time monitoring of harmful algal blooms and turbidity in reservoirs," *JAWRA J. Amer. Water Resour. Assoc.*, vol. 59, no. 5, pp. 929–949, Oct. 2023, doi: 10.1111/1752-1688.13121.

[32] S. M. Power et al., "A novel low-cost plug-and-play multi-spectral LED based fluorometer, with application to chlorophyll detection," *Anal. Methods*, vol. 15, no. 41, pp. 5474–5482, 2023, doi: 10.1039/d3ay00991b.

[33] D. B. Krkljes et al., "Multiparameter water quality monitoring system for continuous monitoring of fresh waters," *IEEE Sensors J.*, vol. 24, no. 7, pp. 11246–11260, Apr. 2024, doi: 10.1109/JSEN.2024.3368560.

[34] *LoRa*. Accessed: Apr. 21, 2024. [Online]. Available: https://lora.readthedocs.io/en/latest/

[35] R. J. Ritchie, "Universal chlorophyll equations for estimating chlorophylls *a*, *b*, *c*, and *d* and total chlorophylls in natural assemblages of photosynthetic organisms using acetone, methanol, or ethanol solvents," *Photosynthetica*, vol. 46, no. 1, pp. 115–126, Mar. 2008, doi: 10.1007/s11099-008-0019-7.

[36] T. Goblirsch, T. Mayer, S. Penzel, M. Rudolph, and H. Borsdorf, "In situ water quality monitoring using an optical multiparameter sensor probe," *Sensors*, vol. 23, no. 23, p. 9545, Nov. 2023, doi: 10.3390/s23239545.